MnO$_x$/Graphene for the Catalytic Oxidation and Adsorption of Elemental Mercury

Haomiao Xu, Zan Qu,* Chenxi Zong, Wenjun Huang, Fuquan Quan, and Naiqiang Yan*

School of Environmental Science and Engineering, Shanghai Jiao Tong University, Shanghai 200240, China

Ⓢ *Supporting Information*

ABSTRACT: MnO$_x$/graphene composites were prepared and employed to enhance the performance of manganese oxide (MnO$_x$) for the capture of elemental mercury (Hg^0) in flue gas. The composites were characterized using FT-IR, XPS, XRD, and TEM, and the results showed that the highly dispersed MnO$_x$ particles could be readily deposited on graphene nanosheets via hydrothermal process described here. Graphene appeared to be an ideal support for MnO$_x$ particles and electron transfer channels in the catalytic oxidation of Hg^0 at a high efficiency. Thus, MnO$_x$/graphene-30% sorbents exhibited an Hg^0 removal efficiency of greater than 90% at 150 °C under 4% O$_2$, compared with the 50% removal efficiency of pure MnO$_x$. The mechanism of Hg^0 capture is discussed, and the main Hg^0 capture mechanisms of MnO$_x$/graphene were catalytic oxidation and adsorption. Mn is the main active site for Hg^0 catalytic oxidation, during which high valence Mn (Mn^{4+} or Mn^{3+}) is converted to low valence Mn (Mn^{3+} or Mn^{2+}). Graphene enhanced the electrical conductivity of MnO$_x$, which is beneficial for catalytic oxidation. Furthermore, MnO$_x$/graphene exhibited an excellent regenerative ability, and is a promising sorbent for capturing Hg^0.
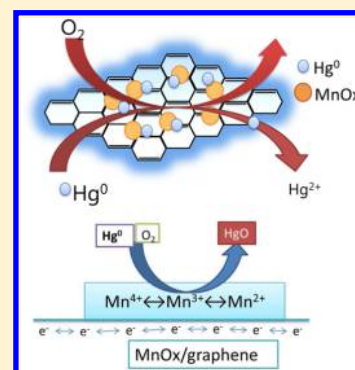
INTRODUCTION

Mercury pollution has attracted significant attention due to its high toxicity in the environment. After years of negotiation via UNEP, the Minamata Convention on Mercury was finally approved in 2013, which aims to reduce worldwide mercury emissions to the environment. It was estimated that approximately 25% ∼ 40% of global mercury is emitted from China annually.[1,2] As the largest producer and consumer of mercury, China has the responsibility of reducing the mercury emissions that are derived from work in various fields.

Coal-fired power plants are the biggest pollution source among the main anthropogenic mercury emission sources.[3] Typically, mercury exists in three forms in coal-fired flue gas: elemental mercury (Hg^0), oxidized mercury (Hg^{2+}) and particulate mercury (Hg^p).[4] Hg^{2+} and Hg^p can be removed by current wet desulfurization devices and dust control units, respectively. However, Hg^0 is difficult to remove with current technologies due to its insolubility in water and volatility.[5] Among various methods of Hg^0 removal, adsorption is considered to be one of the most promising methods, owing to its simplicity and efficiency. So far, the most widely employed sorbent is raw activated carbon due to its structural features, such as its large surface areas and porosity. However, the use of activated carbon for mercury removal still has limitations,[3,6,7] including its expense and lower efficiency for capturing Hg^0. In addition, activated carbon degrades the quality of fly ash and contributes to secondary mercury pollution. Thus, the adverse impacts of activated carbon limit its widespread usages, and it is urgent to find another promising sorbent for Hg^0 capture.

Metal oxide is one potential sorbent due to its low cost and flexible working conditions. Among various metal oxides, manganese oxide (MnO$_x$) has been shown to remove Hg^0 from flue gas effectively through catalytic oxidation and adsorption. The transition metal of Mn offers the ability for Hg^0 oxidation even when there is no HCl in the gas. Yang et al. developed a series of Fe−Mn spinels for capturing Hg^0 and studied the mechanism of adsorption on the surfaces of the sorbents.[8,9] Mn^{4+} active site play an important role in the oxidation of Hg^0. Mn modified fly ash and lignite semicoke were also used to capture Hg^0 capture using Mn active sites.[10,11] However, previous studies have shown that the large size and bulk phase of MnO$_x$ particles hider the full use of the active composites. Several methods have been proposed for the synthesis of MnO$_x$ nanostructures. Nanosize Mn-TiO$_2$ catalysts were synthesized to make full use of the active composites.[12] Zr−Mn binary metal oxide and MnO$_x$-CeO$_2$/TiO$_2$ were also synthesized to enhance the performance of MnO$_x$.[13−15] The capacity of Hg^0 was improved by modifying MnO$_x$ with Zr and Ce, which was attributed to uniform MnO$_x$ particle sizes and oxidation activity. However, these methods often suffer from aggregation and poor conductivity of MnO$_x$ particles, thus reducing their catalytic efficiency. The use of carbon supported MnO$_x$ as catalysts could enhance the conductivity of MnO$_x$, but the porous structure of activated carbon make the sorbent hard to be regenerated.[16]
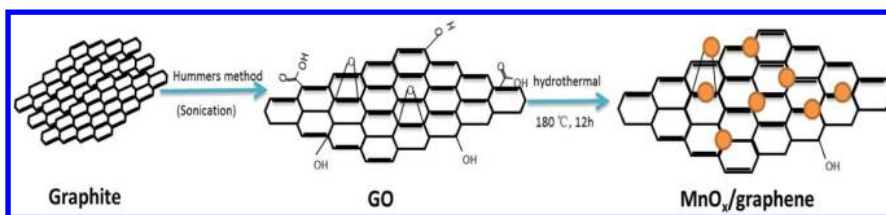
Figure 1. Schematic of synthesis of MnO_x/graphene composites.

Graphene, an emerging material that was first synthesized in 2004, has a single layer of sp^2-bonded carbon atoms packed into a benzene-ring structure and is a nearly ideal 2D material.[17] It is one of the most exciting materials that has been investigated due to its exceptional electrical, mechanical, and thermal properties.[18] Recently, graphene-based materials have been studied for their use in many applications, such as graphene-based composite materials, batteries, chemical detectors and many other areas. However, studies regarding gas purification are lacking. The properties of graphene offer the possibility for modifying MnO_x. The use of graphene could overcome the disadvantages of MnO_x, wherein the large surface area (calculated value, 2630 m^2 g^{-1}) and mobility of charge carriers (200 000 $cm^2 \cdot V^{-1} \cdot s^{-1}$) of graphene make it a good candidate.[19] The structure of graphene is beneficial for the mass transport of gas. Hence, the combination of graphene sheets and MnO_x particles benefit the application of MnO_x metal oxides. From the literature, graphene oxide (GO), the precursor to graphene, plays an important role in the synthesis of graphene based composites. The many functional groups on the GO sheets offer abundant nucleation sites for Mn atoms. Therefore, we prepared our sorbents using an in situ growth technology via a solvothermal route.

Herein, we report a highly economical method for the large-scale synthesis of MnO_x/graphene composites to overcome the problem of particle aggregation and to enhance the electrical conductivity of MnO_x. The composite was investigated for the removal Hg^0 from simulated flue gas. The Hg^0 adsorption experiments were studied using a fix-bed adsorption device at 100 to 300 °C. The oxidation and adsorption mechanism for capturing Hg^0 over MnO_x/graphene are discussed in light of the tests results and characterization techniques.

EXPERIMENTAL SECTION

Preparation of Graphene, MnO_x and MnO_x/Gaphene. Graphene oxide (GO) was synthesized from graphite powder based on the Hummers method.[20] The specific method for the preparation of GO is provided in the Supporting Information. $Mn(NO_3)_2$ (50% w/w), and sodium hydroxide reagents were used to prepare the sorbents's. Ultrapure water was used in each synthesis step.

An economical method was used to prepare the MnO_x/graphene composite. In the first step, as illustrated in Figure 1, a graphene oxide (GO) suspension was produced according to the Hummers method using natural graphite power. GO was used as the precursor of graphene, and Mn particles were grow on its surface. During this process, large quantities of Mn ions favorably bound with the O atoms of the negatively charged oxygen-containing functional groups on the GO sheets via electrostatic forces. Finally, highly dispersed MnO_x nano-particles were deposited in situ and anchored on the surfaces of the graphene to form MnO_x/graphene composites. MnO_x/graphene composites with various mass concentrations of

graphene, MnO_x+graphite-30% and MnO_x+graphene-30%, were also synthesized. (Supporting Information)

Material Characterizations. FTIR spectroscopy was carried out to characterize the surface properties. The micrographs were obtained in the bright-field imaging mode at an acceleration voltage of 120 kV. Power X-ray diffraction (XRD) (APLX-DUO, BRUKER, Germany) data were collected in the 2θ range from 10° to 80° with a scanning velocity of 5°/min using Cu–Kα radiation. The morphologies and nano-structures of MnO_x, graphene and MnO_x/graphene were investigated via transmission electronic microscopy (TEM). TEM images were acquired using a JEOLJEM-2010 TEM. X-ray photoelectron spectroscopy (XPS) was used to analyze the surface characteristics of the sorbents. The XPS system contained an AXIS Ultra DLD (Shimadzu–Kratos) spectrometer with Al Kα as the excitation source. The C 1s line at 284.6 eV was taken as a reference for the binding energy calibration. The electric conductivity of the material was proposed by Hsin et al.[21]

Elemental Mercury (Hg^0) Removal Measurements. A lab-scale fixed-bed adsorption system was assembled, as shown in Supporting Information Figure S1, to explore the uptake capacity of Hg^0 by the sorbents. The fixed-bed reactor was constructed to allow for a total gas flow of 500 mL/min at temperatures from 100 to 300 °C. Fifty milligrams of each sorbent were used for each experiment. During the test, the mercury inlet gas bypassed the sorbent bed and passed into the analytical system until the desired inlet mercury concentration was established. Temperature control devices were installed to control the mixed gas and the reactor temperature. The tests were carried out in the reactor that was maintained at 100−300 °C under Hg^0-laden nitrogen flow. To investigate the effect of temperature on the flue gas, the area under the breakthrough curves corresponding to Hg^0 on the prepared sorbents during the test time (100 min or 10 h) was integrated. To investigate the effects of various gas components, 4% O_2, 500 ppm of SO_2 and 25 ppm of HCl were chosen when needed.

The Hg^0 removal efficiency and the adsorption capacities of Hg^0 were calculated according to eq 1 and eq 2:

$$\eta_r = \frac{Hg^0_{in} - Hg^0_{out}}{Hg^0_{in}} \tag{1}$$

$$Q = \frac{1}{m} \int_{t2}^{t1} (Hg^0_{in} - Hg^0_{out}) \times f \times dt \tag{2}$$

where η_r is the removal efficiency, Q is the Hg^0 adsorption capacity, m is the mass of the sorbent in the fixed-bed, f is the flow rate of the influent, and t_0 and t_1 are the initial and final test times of the breakthrough curves.

To identify the species of mercury in the outlet flue gas, a 10% $SnCl_2$ aqueous solution or a 10% KCl aqueous solution was placed in front of the mercury analyzer. Hg^{2+} was reduced to Hg^0 after passing the $SnCl_2$ solution. The total concentration
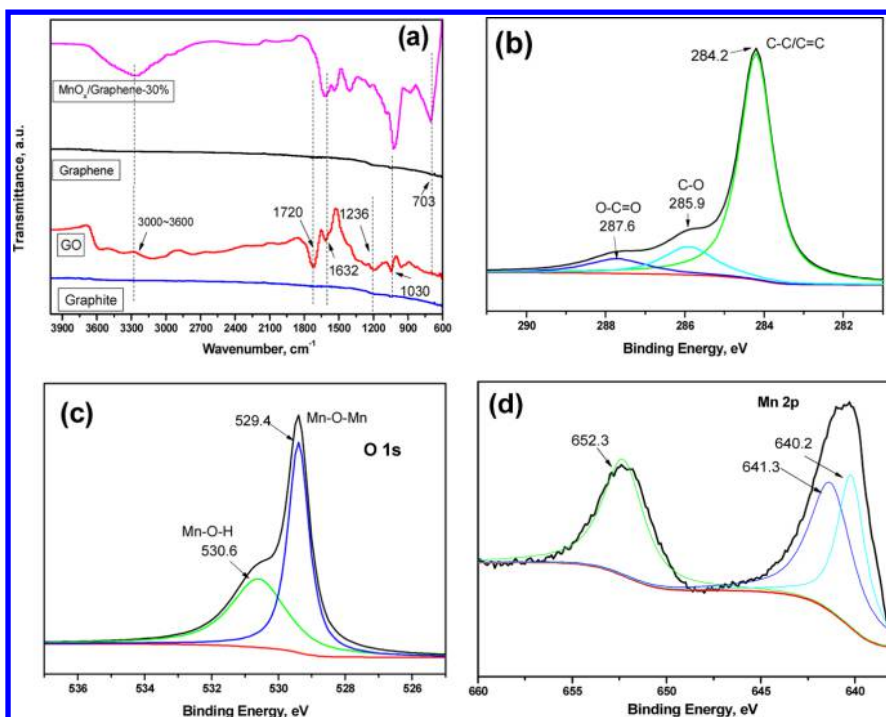
Figure 2. (a) FT-IR spectra and the (b) C 1s, (c) O 1s, and (d) Mn 2p XPS spectra of the MnO_x/graphene-30% composite.
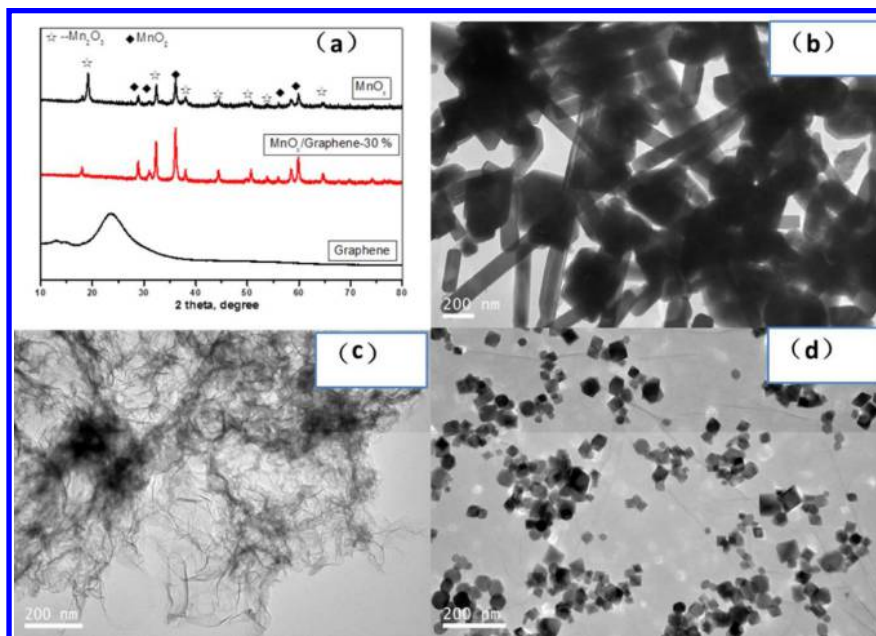
Figure 3. (a) XRD patterns of MnO_x, graphene and MnO_x/graphene-30%; TEM images of (b) MnO_x, (c) graphene, and (d) MnO_x/graphene-30%.

of mercury (Hg^T) was measured with the simulated flue gas passing through a $SnCl_2$ solution. Herein, the Hg^0 oxidation efficiency (η_o) can be defined as follows:

$$\eta_o = \frac{Hg^T_{out} - Hg^0_{out}}{Hg^0_{in}} \qquad (3)$$

Sorbents Regeneration. A mercury-temperature-programmed desorption (Hg-TPD) method was designed to investigate the regeneration characteristics of the sorbents.[22] After mercury adsorption at 150 °C with 4% O_2 for 30 min, the sorbents were regenerated by heating from 100 to 500 °C in a

pure N_2 carrier gas. Hg-TPD curves under different heating rates (2 °C/min, 5 °C/min and 10 °C/min) on the MnO_x/graphene surfaces were collected. The desorption activation energy was also calculated according to the results.

■ RESULTS AND DISCUSSION

Characterization of the Materials. To investigate the chemical structure of the prepared samples, the FT-IR spectra were characterized. Figure 2 (a) shows the spectra of graphite, GO, graphene and MnO_x/graphene-30%. In the case of GO, peaks appeared at the C=O (1720 cm^{-1}), the aromatic C=C (1632 cm^{-1}), the epoxy C−O (1236 cm^{-1}), and the alkoxy C−
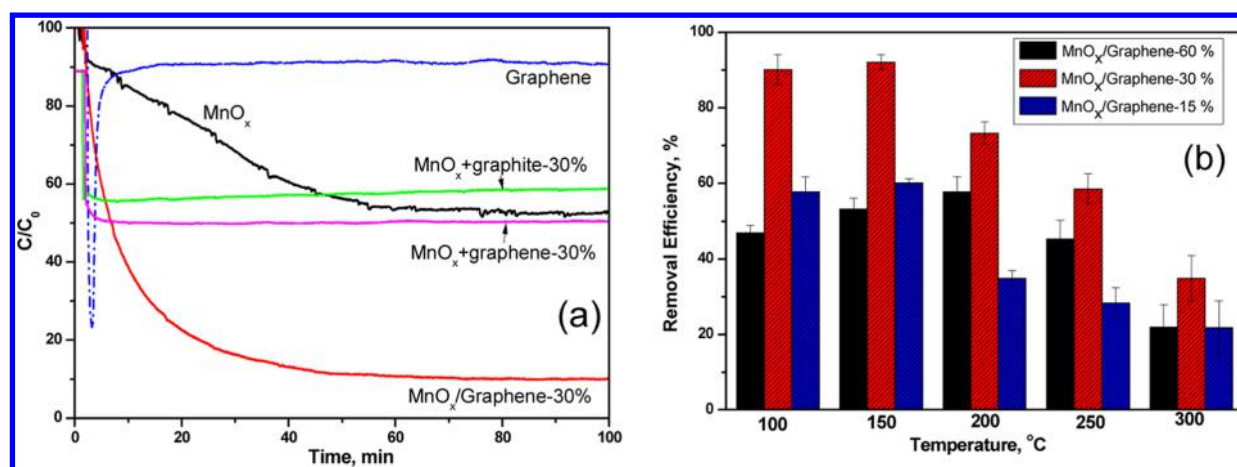
Figure 4. (a) The performance of prepared sorbents at 150 °C under 4% O_2. (b) The Hg^0 removal efficiency of various mass percentages of graphene at different temperatures under 4% O_2 (10 h adsorption).

O (1030 cm^{-1}) stretching vibrations. The broad band at approximately 3000−3600 cm^{-1} corresponds to the vibrations of the absorbed water molecules. After hydrothermal reduction, the function peaks disappeared according to the spectrum of graphene. For the MnO_x/graphene composites, the peaks of C=O and epoxy C−O diminished, which indicated removal of the oxy-functional groups after hydrothermal treatment. A new peak at 703 cm^{-1} was attributed to the vibration of the Mn−O−C bond.[23] The FT-IR results confirm the successful integration of Mn atoms on graphene.

XPS was also performed to further illustrate the chemical composition of the MnO_x/graphene-30% composite. The Mn 2p spectrum is presented in Figure 2 (d), where the peaks at 641.3 and 640.2 eV correspond to Mn^{4+} and Mn^{3+}, respectively. Regarding oxygen (Figure 2 (c), two peaks at 529.4 and 530.6 eV correspond to Mn−O−Mn and Mn−O−H, respectively.[24] Therefore, Mn atoms may interact with the O atoms of the residual functional groups on GO sheets via a covalent coordination bond or a hydrogen bond. Figure 2 (b) shows the C 1s spectrum of MnO_x/graphene-30%. The three peaks at 284.2, 285.9, and 287.6 eV in the C 1s spectrum correspond to C−C/C=C groups in aromatic rings, C−O groups (epoxy and alkoxy), and O−C=O groups, respectively.[25] The predominant C−C/C=C functional groups guarantee good electrical conductivity of the composite.[26]

Figure 3 shows the XRD patterns and the TEM images of the prepared samples. The XRD patterns are shown in Figure 3(a). An obvious peak at approximately 20−30° for graphene indicated that the graphene structure was successfully synthesized in our experiment.[27] For MnO_x, several diffraction peaks were detected that were ascribed to Mn_2O_3 (PDF 24−0508) and MnO_2 (PDF 65-2861). After graphene was wrapped, the diffraction line of MnO_x became more apparent and intense, which could be attribute to the change in particle size and the formation of more uniform particles. Furthermore, the pattern of graphene was not apparent in the MnO_x/graphene-30% samples. It was possible that MnO_x dispersed on the surface of graphene or graphene sheets were inserted into the MnOx particles due to the high intensity of MnO_x.

TEM characterization provides a convenient approach to investigate the morphology of graphene, MnO_x and MnO_x/graphene-30%. Images of two microscopic MnO_x morphologies are shown in Figure 3 (b), rod-like and particle-like MnO_x, which highly aggregate in the absence of graphene. Pure

graphene sheets after the thermal reduction of GO are shown in Figure 3 (c). The synthesized graphene sheets were quite thin and consisted only of a few carbon layers. Figure 3(d) shows images of MnO_x/graphene-30%, revealing that the MnO_x particles deposited on the surface of the graphene sheets and that the MnO_x particles became smaller. MnO_x nanoparticles with a size of approximately 10−20 nm were found uniformly distributed the graphene structure. Most of the graphene sheets were embedded in the MnO_x particles, which suggests that the graphene sheets were inserted into the bulk of the MnO_x particles.[28] Furthermore, the TEM images of MnO_x+graphite-30% and MnO_x+graphene-30% are shown in Supporting Information Figure S2 for comparison. The image of MnO_x+graphite-30% shows that the MnO_x particles became smaller compared to the MnO_x particles, but that the particles were still massive, and that the particles and graphite were independent of one other. Regarding MnO_x+graphene-30%, the graphene and the MnO_x particles appeared to be mixed together, and the MnO_x particles were large and uniform in size. Such results indicate that graphene can prevent the aggregation of MnO_x particles. This result could be ascribed to the MnO_x nanoparticles grown on GO through functional groups, such as carboxyl, hydroxyl, and epoxy groups.[29] Thus, the highly dispersed nanoscale MnO_x particles increased the catalytic activity.

The Performance of the Prepared Materials. The prepared materials were studied for their ability to capture Hg^0 on a fix-bed device. The Hg^0 removal efficiency of MnO_x, graphene and MnO_x/graphene-30% at a temperature of 150 °C with 4% O_2 are presented in Figure 4 (a). MnO_x+graphite-30% and MnO_x+graphene30% were also tested for comparison. Graphene alone appeared to be inert to Hg^0 removal. A removal efficiency less than 50% was obtained for MnO_x. The removal efficiencies of MnO_x+graphite-30% and MnO_x+graphene30% were approximately 50% and 43%, respectively. Mechanical interactions between the MnO_x particles did not contribute the Hg^0 removal efficiency. For the MnO_x/graphene-30% sample, the Hg^0 removal efficiency exceeded 90%. Based on the TEM and XPS analyses, the increase in adsorption performance was attributed to more Mn active sites on the surface of the graphene. Graphene nanosheets can prevent the aggregation of MnO_x particles and serve as electron transfer channels.[29] The chemical
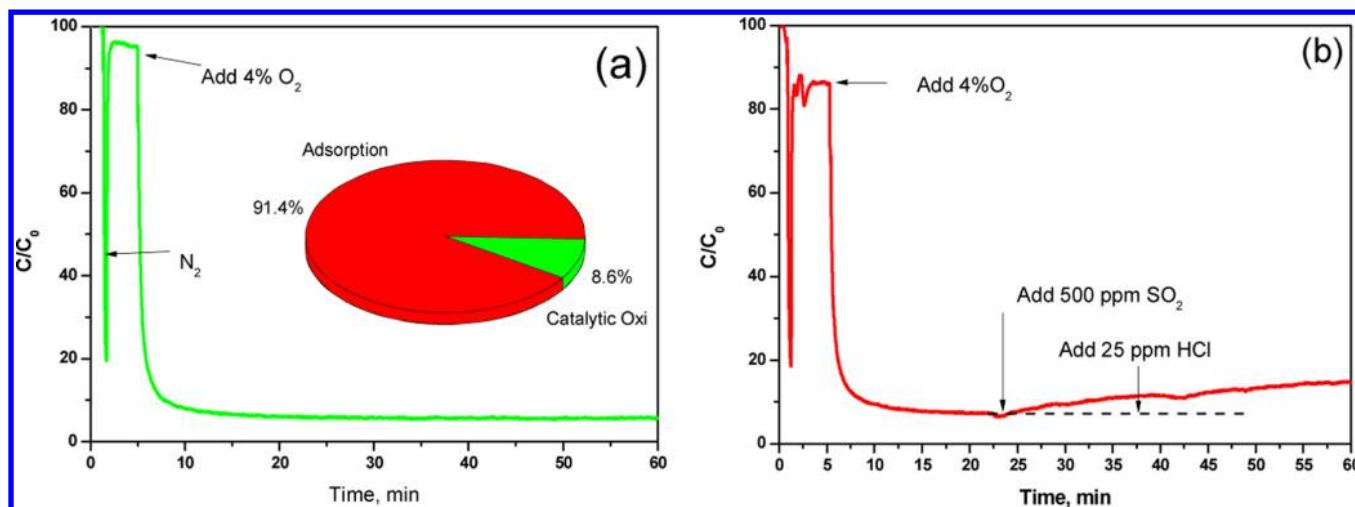
Figure 5. (a) Effect of O_2. (b) Effect of SO_2 and HCl (150 °C).
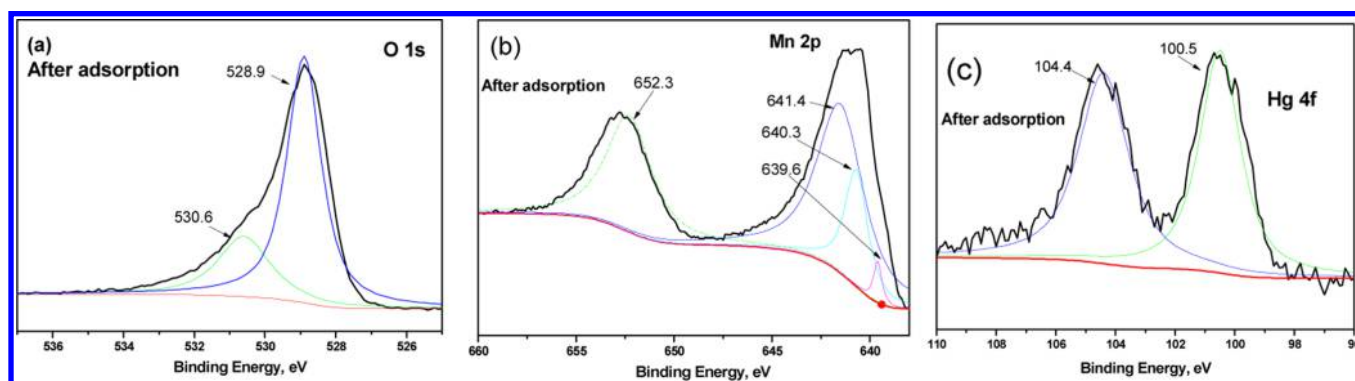
Figure 6. XPS spectra of MnO_x/graphene-30% after adsorption for (a) O 1s, (b) Mn 2p, and (c) Hg 4f.

interactions between MnO_x and graphene significantly improve the adsorption behavior compared to MnO_x alone.

Furthermore, the effect of the mass ratios of graphene to MnO_x over a range of temperatures from 100 to 300 °C were investigated, and the results are shown in Figure 4 (b). The composite containing the 30% graphene at 150 °C yielded the highest removal efficiency. The removal efficiency significantly decreased when the mass percentage of graphene in the composites was increased from 30% to 60%. The capacity of MnO_x/graphene-30% for 10 h adsorption yielded up to 2.7 mg/g of captured Hg. The high removal efficiency of MnO_x/graphene-30% further indicated that the main active sites for Hg^0 capture were MnO_x. MnO_x/graphene-30% showed better performance than MnO_x was due to the high dispersion of MnO_x particles. Furthermore, the electrical conductivity of MnO_x was enhanced when added graphene. The results in Supporting Information Table S2 showed that the value of MnO_x was not detected because the resistance was over range. The electrical conductivity of graphene and MnOx/graphene-30% were 228.3 and 2.14 S/m, respectively. The electrical conductivity of MnO_x was enhanced due to the higher conductivity of graphene.

Adsorption and Oxidization of Hg^0 over MnO_x/Graphene. Based on the results shown in Figure 4, the MnO_x/graphene-30% composite exhibited the best performance for the removal of Hg^0 under 4% O_2. According to the previous studies, it was believed that Hg^0 could be oxidized over the MnO_x catalyst.[4] Additionally, SO_2 and HCl were the

primary components in the flue gas in this study, and the effect of these acidic gases was also considered. Figure 5 (a) shows the effect of O_2 over the MnO_x/graphene-30% sorbent. As expected, there was almost negligible Hg^0 removal when no O_2 was present. However, the removal efficiency exceeded 90% when 4% O_2 was added to the mixed gas. To further investigate the catalytic oxidation of Hg^0, the Hg^0 oxidation efficiency (η_o) was calculated. η_o was approximately 8.6% for the total Hg^0 removal. Here, most of the mercury was taken up on the surface of MnO_x/graphene-30% during the adsorption process.

SO_2 and HCl are the two main constituents in real flue gas and are often discussed regarding their impact in Hg^0 oxidation.[30] As shown in Figure 5 (b), the addition of 25 ppm of HCl made no difference in the removal of Hg^0. Notably, the sorbent could be used when the concentration of HCl in the simulated gas was low. However, when 500 ppm of SO_2 was added to the simulated gas, the removal efficiency was gradually decreased by approximately 10%. It can be speculated that a competitive adsorption for MnO_x exists between SO_2 and Hg^0.[22]

As demonstrated in the adsorption test, MnO_x/graphene-30% exhibited excellent Hg^0 adsorption performance. To better understand the Hg^0 adsorption mechanisms, the XPS spectra of Hg^0 adsorption at 150 °C were compared. As shown in Figure 6, the XPS spectra over the regions of O 1s, Mn 2p, and Hg 4f are given. Figure 6 (a) shows the spectrum of O 1s in which one peak at 528.9 eV corresponds to the lattice oxygen of MnO_x and another peak at 530.6 eV corresponds to the
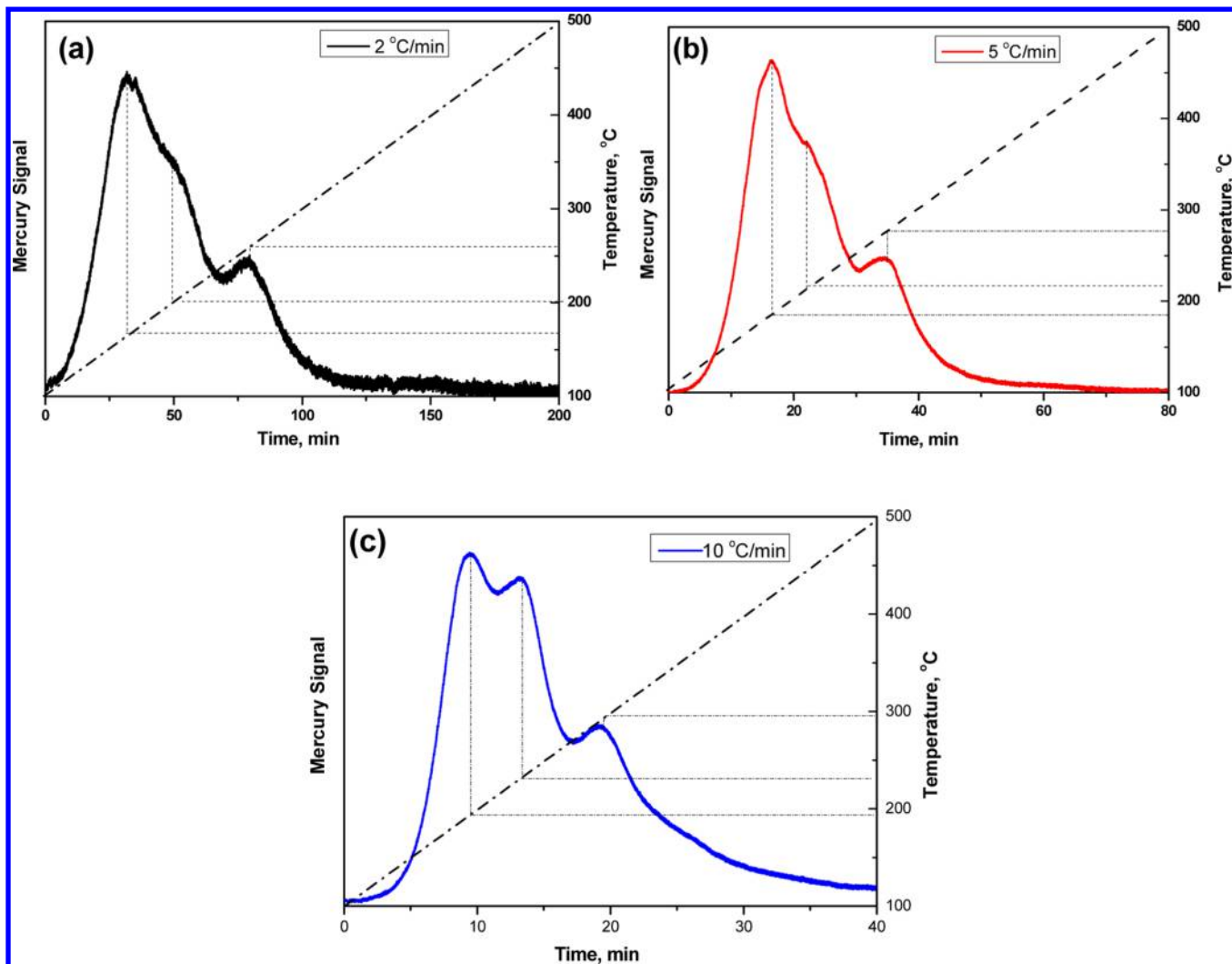
Figure 7. Hg-TPD curves of MnO$_x$/graphene-30% at different rates of heating.

hydroxyl oxygen. After the adsorption test, there was an increase in the lattice oxygen compared to that shown in Figure 6 (a). This observation suggested that oxygen took part in the reaction during the adsorption process. The XPS results of Mn 2p are shown in Figure 6 (b), the peaks at 641.4, 640.3, and 639.6 eV correspond to Mn^{4+}, Mn^{3+} and Mn^{2+}, respectively. After the adsorption at 150 °C, a peak corresponding to Mn^{2+} was observed. This could be due to the occurrence of a reduction reaction on the surface of the MnO$_x$/graphene-30%. In addition, the molar ratio of Mn^{4+} to Mn^{3+} increased in the spectra. It is believed that O$_2$ plays an important role in the oxidation of Mn^{3+}. The XPS spectrum of Hg 4f is also shown in Figure 6 (c) for comparison. The characteristic peaks at 100.5 and 104.4 eV correspond to Hg 4f 7/2 and Hg 4f 5/2, respectively, and were assigned to HgO. This indicated that the main species of mercury was HgO on the surface of MnO$_x$/graphene.

From the above studies, the adsorption mechanism of Hg^0 can be described as follows ([O] represent the lattice oxygen):[4]

$$Hg(g) \rightarrow Hg(ads) \tag{4}$$

$$2MnO_2 \rightarrow Mn_2O_3 + [O] \tag{5}$$

$$Mn_2O_3 \rightarrow 2MnO + [O] \tag{6}$$

$$[O] + Hg(ads) \rightarrow HgO(ads) \tag{7}$$

$$MnO + \frac{1}{2}O_2 \rightarrow MnO_2 \tag{8}$$

$$Mn_2O_3 + \frac{1}{2}O_2 \rightarrow 2MnO_2 \tag{9}$$
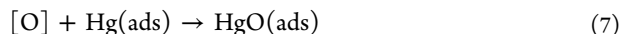
In the adsorption process, Hg^0 adsorption on MnO$_x$/graphene is a dynamic process: first the Hg^0(g) forms Hg(ads), then MnO$_2$ and Mn$_2$O$_3$ offer the lattice oxygen for the oxidation of Hg(ads). The reduced Mn$_2$O$_3$ and MnO can be converted back to their original state by O$_2$ in the gas. Graphene enhances the electrical conductivity of pure MnO$_x$ by improving the electron transfer on the graphene nanosheets.[31] Hg^0 was collected on the surface of MnO$_x$/graphene.

Regeneration. Furthermore, the property of regeneration was tested using the Hg-TPD method, and the activation energy for desorption was calculated. The results of the Hg-TPD curves under different rates of heating on MnO$_x$/graphene-30% are shown in Figure 7. During the desorption process at each heating rate, three peaks emerged on the Hg-TPD curves, suggesting that three forms of existing mercury combined with MnO$_x$. The appearance of desorption peaks at higher temperatures indicate stronger interaction forces

between the mercury and adsorption sites. According to the results, mercury could be released at temperatures higher than 160 °C under pure N_2 conditions, a notable result for sorbent regeneration at such low temperature. The low activation energy for desorption could be beneficial for regeneration. Based on the desorption data under different rates of heating, the desorption activation energy was calculated according to eq 10.

$$2 Ln T_p - Ln \beta = \frac{E_d}{R T_p} + Ln \frac{E_d}{AR} \tag{10}$$

where T_p is the maximum value at a certain temperature (K), β is the heating rate (K/min), E_d is the desorption activation energy (kJ/mol), R is the gas constant, T is the temperature (K), and A is a pre-exponential factor.

According to the equation, the desorption activation energies of peak 1, peak 2, and peak 3 were 58.31 kJ/mol, 71.28 kJ/mol, and 86.38 kJ/mol, respectively (Supporting Information Table S1). The desorption activation energy of peak 1 corresponding to pure MnO_x was also calculated according to the Hg-TPD curves (Supporting Information Figure S3) and was lower than the energy of pure MnO_x (109.34 kJ/mol). Mercury could be released from the surface of MnO_x/graphene-30% via a simple thermal method. The regenerative ability of MnO_x/graphene highlights its potential for future applications.

In summary, a series of MnO_x constructs on graphene were successfully prepared via a deposition precipitation method. The MnO_x/graphene-30% composite exhibited better performance for capturing Hg^0 than the pure MnO_x sorbent due to the highly dispersed MnO_x particles on the graphene nanosheets. The small-sized and uniform MnO_x nanoparticles decorated the graphene nanosheets. The nanosheets showed high electrical conductivity, which is beneficial for Hg^0 oxidation. The regeneration experiments showed that the deposition precipitation method was an environmentally sound process, based on the promising performance for regeneration.

ASSOCIATED CONTENT

Ⓢ Supporting Information
The GO and MnO_x/graphene composite synthesis methods, Hg0 capacity assessment system, TEM images, Hg-TPD results and calculation of mercury desorption activation energy from the MnO_x/graphene-30% surface are provided. The Supporting Information is available free of charge on the ACS Publications website at DOI: 10.1021/es505978n.

AUTHOR INFORMATION

Corresponding Authors
*Phone: +86 21 54745591; fax: +86 21 54745591; e-mail: quzan@sjtu.edu.cn (Z.Q.).
*Phone: +86 21 54745591; fax: +86 21 54745591; e-mail: nqyan@sjtu.edu.cn (N.Y.).

Notes
The authors declare no competing financial interest.

REFERENCES

(1) Wang, S.; Zhang, L.; Wang, L.; Wu, Q.; Wang, F.; Hao, J. A review of atmospheric mercury emissions, pollution and control in China. *Front. Environ. Sci. Eng.* **2014**, *8* (5), 631−649.

(2) Fu, X.; Feng, X.; Sommar, J.; Wang, S. A review of studies on atmospheric mercury in China. *Sci. Total Environ.* **2012**, *421*, 73−81.

(3) Pavlish, J. H.; Sondreal, E. A.; Mann, M. D.; Olson, E. S.; Galbreath, K. C.; Laudal, D. L.; Benson, S. A. Status review of mercury control options for coal-fired power plants. *Fuel Process. Technol.* **2003**, *82* (2−3), 89−165.

(4) Presto, A. A.; Granite, E. J. Survey of catalysts for oxidation of mercury in flue gas. *Environ. Sci. Technol.* **2006**, *40* (18), 5601−5609.

(5) Driscoll, C. T.; Mason, R. P.; Chan, H. M.; Jacob, D. J.; Pirrone, N. Mercury as a global pollutant: Sources, pathways, and effects. *Environ. Sci. Technol.* **2013**, *47* (10), 4967−4983.

(6) Tan, Z.; Sun, L.; Xiang, J.; Zeng, H.; Liu, Z.; Hu, S.; Qiu, J. Gas-phase elemental mercury removal by novel carbon-based sorbents. *Carbon* **2012**, *50* (2), 362−371.

(7) Li, Y. H.; Lee, C. W.; Gullett, B. K. Importance of activated carbon's oxygen surface functional groups on elemental mercury adsorption. *Fuel* **2003**, *82* (4), 451−457.

(8) Yang, S.; Guo, Y.; Yan, N.; Qu, Z.; Xie, J.; Yang, C.; Jia, J. Capture of gaseous elemental mercury from flue gas using a magnetic and sulfur poisoning resistant sorbent Mn/gamma-Fe2O3 at lower temperatures. *J. Hazard. Mater.* **2011**, *186* (1), 508−515.

(9) Yang, S.; Guo, Y.; Yan, N.; Wu, D.; He, H.; Xie, J.; Qu, Z.; Jia, J. Remarkable effect of the incorporation of titanium on the catalytic activity and SO2 poisoning resistance of magnetic Mn-Fe spinel for elemental mercury capture. *Appl. Catal., B* **2011**, *101* (3−4), 698−708.

(10) Xing, L.; Xu, Y.; Zhong, Q. Mn and Fe modified fly ash as a superior catalyst for elemental mercury capture under air conditions. *Energy Fuels* **2012**, *26* (8), 4903−4909.

(11) Zhang, H.; Chen, J.; Liang, P.; Wang, L. Mercury oxidation and adsorption characteristics of potassium permanganate modified lignite semi-coke. *J. Environ. Sci. (Beijing, China)* **2012**, *24* (12), 2083−2090.

(12) Xie, J.; Yan, N.; Yang, S.; Qu, Z.; Chen, W.; Zhang, W.; Li, K.; Liu, P.; Jia, J. Synthesis and characterization of nano-sized Mn-TiO2 catalysts and their application to removal of gaseous elemental mercury. *Res. Chem. Intermed.* **2012**, *38* (9), 2511−2522.

(13) Xie, J.; Qu, Z.; Yan, N.; Yang, S.; Chen, W.; Hu, L.; Huang, W.; Liu, P. Novel regenerable sorbent based on Zr-Mn binary metal oxides for flue gas mercury retention and recovery. *J. Hazard. Mater.* **2013**, *261*, 206−213.

(14) Li, H.; Wu, C.-Y.; Li, Y.; Zhang, J. Superior activity of MnO_x-CeO2/TiO2 catalyst for catalytic oxidation of elemental mercury at low flue gas temperatures. *Appl. Catal., B* **2012**, *111*, 381−388.

(15) He, C.; Shen, B.; Chen, J.; Cai, J. Adsorption and oxidation of elemental mercury over Ce-MnO_x/Ti-PILCs. *Environ. Sci. Technol.* **2014**, *48* (14), 7891−7898.

(16) Mei, Z.; Shen, Z.; Zhao, Q.; Wang, W.; Zhang, Y. Removal and recovery of gas-phase element mercury by metal oxide-loaded activated carbon. *J. Hazard. Mater.* **2008**, *152* (2), 721−729.

(17) Novoselov, K. S.; Geim, A. K.; Morozov, S. V.; Jiang, D.; Zhang, Y.; Dubonos, S. V.; Grigorieva, I. V.; Firsov, A. A. Electric field effect in atomically thin carbon films. *Science* **2004**, *306* (5696), 666−669.

(18) Georgakilas, V.; Otyepka, M.; Bourlinos, A. B.; Chandra, V.; Kim, N.; Kemp, K. C.; Hobza, P.; Zboril, R.; Kim, K. S. Functionalization of graphene: Covalent and non-covalent approaches, derivatives and applications. *Chem. Rev.* **2012**, *112* (11), 6156−6214.

(19) Park, S.; Ruoff, R. S. Chemical methods for the production of graphenes. *Nat. Nanotechnol.* **2009**, *4* (4), 217−224.

(20) Marcano, D. C.; Kosynkin, D. V.; Berlin, J. M.; Sinitskii, A.; Sun, Z.; Slesarev, A.; Alemany, L. B.; Lu, W.; Tour, J. M. Improved synthesis of graphene oxide. *ACS Nano* **2010**, *4* (8), 4806−4814.

(21) Hsin, Y. L.; Hwang, K. C.; Yeh, C.-T. Poly (vinylpyrrolidone)-modified graphite carbon nanofibers as promising supports for PtRu catalysts in direct methanol fuel cells. *J. Am. Chem. Soc.* **2007**, *129* (32), 9999−10010.

(22) Xie, J.; Xu, H.; Qu, Z.; Huang, W.; Chen, W.; Ma, Y.; Zhao, S.; Liu, P.; Yan, N. Sn-Mn binary metal oxides as non-carbon sorbent for mercury removal in a wide-temperature window. *J. Colloid Interface Sci.* **2014**, *428*, 121−127.

(23) Hu, M.; Hui, K.; Hui, K. Role of graphene in MnO_2/graphene composite for catalytic ozonation of gaseous toluene. *Chemical Engineering Journal* **2014**, *254*, 237−244.

(24) Lei, Z.; Shi, F.; Lu, L. Incorporation of MnO_2-coated carbon nanotubes between graphene sheets as supercapacitor electrode. *ACS Appl. Mater. Interfaces* **2012**, *4* (2), 1058−1064.

(25) Jiangying, Q.; Lin, S.; Chunxiang, H.; Feng, G.; Beibei, L.; Quan, Z.; Han, H.; Guanghua, S.; Xuzhen, W.; Jieshan, Q. Highly efficient synthesis of graphene/MnO_2 hybrids and their application for ultrafast oxidative decomposition of methylene blue. *Carbon* **2014**, *66*, 485−92.

(26) Chen, S.; Zhu, J.; Wu, X.; Han, Q.; Wang, X. Graphene oxide−MnO_2 nanocomposites for supercapacitors. *ACS Nano* **2010**, *4* (5), 2822−2830.

(27) Gu, Y.; Xu, Y.; Wang, Y. Graphene-wrapped CoS nanoparticles for high-capacity lithium-ion storage. *ACS Appl. Mater. Interfaces* **2013**, *5* (3), 801−806.

(28) Niu, T.; Liu, G. L.; Liu, Y. Preparation of Ru/graphene-meso-macroporous SiO_2 composite and their application to the preferential oxidation of CO in H_2-rich gases. *Appl. Catal., B* **2014**, *154*, 82−92.

(29) Wang, H.; Cui, L.-F.; Yang, Y.; Casalongue, H. S.; Robinson, J. T.; Liang, Y.; Cui, Y.; Dai, H. Mn_3O_4-graphene hybrid as a high-capacity anode material for lithium ion batteries. *J. Am. Chem. Soc.* **2010**, *132* (40), 13978−13980.

(30) Li, Y.; Murphy, P.; Wua, C.-Y. Removal of elemental mercury from simulated coal-combustion flue gas using a SiO_2-TiO_2 nano-composite. *Fuel Process. Technol.* **2008**, *89* (6), 567−573.

(31) Yang, Q.; Li, Q.; Yan, Z.; Hu, X.; Kang, L.; Lei, Z.; Liu, Z.-H. High performance graphene/manganese oxide hybrid electrode with flexible holey structure. *Electrochim. Acta* **2014**, *129*, 237−244.